

Towards Passive Safe Reinforcement Learning: A Comparative Study on Contact-rich Robotic Manipulation

Heng Zhang^{1,2}, Gokhan Solak¹, Sebastian Hjorth¹, Arash Ajoudani¹

Abstract—Reinforcement learning (RL) has achieved remarkable success in various robotic tasks; however, its deployment in real-world scenarios, particularly in contact-rich environments, often overlooks critical safety and stability aspects. Policies without passivity guarantees can result in system instability, posing risks to robots, their environments, and human operators. In this work, we investigate the limitations of traditional RL policies when deployed in contact-rich tasks and explore the combination of energy-based passive control with safe RL in both training and deployment to answer these challenges. Firstly, we introduce energy-based constraints in our safe RL formulation to train *passivity-aware* RL agents. Secondly, we add a passivity filter on the agent output for *passivity-ensured* control during deployment. We conduct comparative studies on a contact-rich robotic maze exploration task, evaluating the effects of learning passivity-aware policies and the importance of passivity-ensured control. The experiments demonstrate that a passivity-agnostic RL policy easily violates energy constraints in deployment, even though it achieves high task completion in training. The results show that our proposed approach guarantees control stability through passivity filtering and improves the energy efficiency through passivity-aware training. A video of real-world experiments is available as supplementary material. We also release the checkpoint model and offline data for pre-training at [Hugging Face](#)

I. INTRODUCTION

In recent years, RL has earned increasing attention and success in addressing complex decision-making and control problems, especially in robotic applications [1]. From manipulation tasks to autonomous navigation, RL offers the potential to achieve unprecedented performance by learning optimal control policies. However, while RL excels in simulated environments, deploying these policies in real-world robotic systems remains a significant challenge [2]. This is particularly important in contact-rich tasks. Contact-rich tasks require the robots to interact with their environment in a safe and stable manner. Safety, particularly in terms of contact force regulation, is necessary to avoid damaging the environment, the robot, or the objects involved in the task. Stability, on the other hand, is crucial for maintaining predictable and controllable robot behavior, especially when interacting with complex and unpredictable surroundings [3]. For instance, an RL policy trained without considering system stability might generate control commands that cause high-frequency vibrations, or unbounded energy accumulation. Such behaviors can damage the robot, compromise

the task outcome or pose safety risks to humans. Despite these risks, a substantial portion of RL research focuses primarily on maximizing task success rates or improving learning efficiency, with limited attention given to safety and stability. This gap presents a significant barrier to real-world deployment, where stability and safety are not only desirable but essential [4].

Traditional RL policies are often trained and tested in simulated environments without considering stability. This can not be ignored when deployed in real-world robotic tasks [1] since uncertainties and risks in realistic applications often cannot be eliminated. Moreover, contact-rich tasks amplify this risk due to the dynamic and sensitive nature of the interactions involved. Hence, ensuring that RL policies are inherently stable and safe during training and deployment is not only a theoretical concern but a practical necessity for robotics.

The safe RL concept has emerged to answer the safety concerns about the RL policies. Safe RL methods specify the safety requirements usually as constraints and aim to satisfy them while also solving the task [2]. The system can learn to avoid constraints by learning to predict the risk of states and actions from data [5]. In contact-rich tasks, self-proven control concepts such as variable impedance control (VIC) are used to add compliance to the system. A recent work [6] proposed a VIC-based safe RL method that effectively solves the contact-rich maze exploration problem. However, that work focused only on contact-related safety criteria, ignoring the control stability. In this work, we address this limitation by introducing passivity-based control.

Passivity is a fundamental concept in control theory. As proven in [7], passivity-based control is needed to facilitate physical interactions with the environment. It is vital to monitor and restrict the amount of energy allowed to be stored and injected by the controller into the robot to ensure the passivity and safety of the system [8]. Energy tanks are widely used to achieve passivity-based control by restricting the amount of energy allowed to be stored in the system [9], [10].

In the RL literature, the energy tanks were mostly limited to a deployment-time filtering step [11]. To the best of our knowledge, only [12] employed the classical energy-tank based passivity approach during RL training for contact-rich tasks by filtering the RL output and terminating the training episode when the tank is depleted. We advance the prior work by exploring *passivity-aware* learning by explicitly defining passivity-related constraints as part of the RL problem formulation. Leveraging a safe RL framework, we

¹ Human-Robot Interfaces and Interaction Lab, Istituto Italiano di Tecnologia, Genoa, Italy. e-mails: heng.zhang@iit.it

² Ph.D. program of national interest in Robotics and Intelligent Machines (DRIM) and Università di Genova, Genoa, Italy.

This work was supported by the European Union Horizon Project TORNADO (GA 101189557).

simultaneously answer the contact-rich safety and passivity problems. Furthermore, as stated in [13], solely limiting the total amount of energy is insufficient to ensure the passivity of the system. Hence, we augment the energy tank with a flow limit, unlike [12].

In summary, it can be concluded that while current safe RL methods can be utilized for learning control parameters of a VIC by maximizing rewards, the lack of the inclusion of passivity-based control formulations during deployment makes them ill-suited for contact-rich tasks. However, designing an augmented energy tank in terms of size and flow limits for contact-rich tasks is not trivial since the severity and frequency of unplanned interaction can affect energy spending, resulting in a premature depletion of the energy tank at which the task is entirely lost. Including such a tank in the training of the RL agent could lead to an improvement in the design process of augmented energy tanks as well as the overall performance during the deployment phase. Therefore, the presented work focuses on an augmented energy tank-based passivity formalism during the RL training phase to tackle the aforementioned challenges. More specifically, the formalism takes basis from the Safe-RL approach presented in [6] and an augmented global energy tank-based approach inspired by [13] to ensure the passivity of the system. Furthermore, the presented work investigates the effect of such passivity-based formalism on the training/learning phase of the policy. Moreover, the performance in terms of task completion and energy expenditure of the different policies is compared to each other during deployment in simulation and the real world.

To summarize, the novel contributions of the manuscript are the following:

- 1) Investigation of RL policy stability: We analyze the limitation of traditional RL policies that lack passivity guarantees, especially deployed in complex scenarios, demonstrating their poor performance in contact-rich tasks.
- 2) Extensive study of different augmented energy-tank-based designs' effects on the training of a RL policy: We introduce energy-tank-based constraints together with a contact force constraint to train passive safe RL policy.
- 3) Through extensive experiments both in simulation and the real world, we validate the effectiveness of our passivity-aware RL policy and passivity-ensured controller in contact-rich robotic tasks.

II. RELATED WORK

A. Passivity in robot compliant control

In order to facilitate physical interactions with the environment, it was formally proven in [7] that passivity-based control is needed. This becomes even more critical for kinematically redundant robots, as internal motions within the null space of the task Jacobian can result in an unintended increase in system energy, potentially leading to instability. Moreover, it was highlighted in [8] that it is vital to monitor and restrict the amount of energy allowed to be stored

and injected by the controller into the robot to ensure the passivity and safety of the system. One used approach to guarantee passivity are energy tanks. However, as mentioned above and pointed out in [13], the bounding of the energy alone is not sufficient to ensure the passivity of the system, but also the energy flow between the controller and robot has to be limited. In recent years, works such as [14], [9], [10] have focused on restricting the energy flow with the energy tanks.

B. Safe RL for contact-rich robotic tasks

RL can solve challenging contact-rich tasks [15]. In contact-rich tasks, VIC has proven to be an effective solution [16]. Reinforcement Learning (RL) can be leveraged to learn adaptive and safe VIC policies, enabling robust performance in more complex contact-rich scenarios. Specifically, some approaches [17], [18], [19] incorporate VIC parameters directly into the action space by utilizing demonstrations. Using Cartesian VIC as the RL action-space is shown to be effective for contact-rich tasks [20]. However, these works do not explicitly address the safety issues. The safety can be formulated by introducing constraints to the RL policy in the form of a constrained Markov decision process (CMDP) [21]. A way to solve CMDPs is by training a *safety critic* to predict a potential risk value before taking action and train a conservative policy [22]. [5] proposed a recovery mechanism by training a recovery policy to enhance safety. Instead of collision-avoidance as in [5], a recent work [6] integrates a safety critic for contact-rich tasks, by focusing on how to stay safe during and after a collision without sacrificing task completion. However, safe RL policies for contact-rich tasks rarely consider the system's stability, which is essential in real-world deployment. We take a step towards a passive safe RL policy for robotic contact-rich tasks that achieve dual safe and stable performance.

C. Passivity considerations in RL

A passive RL policy can provide benefits in terms of stability and task performance. Work such as [11], [23] uses an RL-based method to train a passive policy; however, the safety issue was not addressed, and the passivity guarantee is more complex in model-agnostic environment [23]. Zanella et al. [12] use an energy tank-based filter to enforce passivity in learned policies. However, their approach is validated only in simulation while ensuring passive performance in real-world deployment remains crucial. In addition, the utilization of an energy tank with the augmented flow limit at its port was not investigated in [12], which is also necessary to bind the energy flow between the controller and robot as mentioned in [13]. Different from the previous research, we go further based on a Safe RL method by not only extending it with passivity-aware RL policy training but also with passivity-ensured deployment in real-world contact-rich tasks.

III. PASSIVE SAFE REINFORCEMENT LEARNING

The presented approach draws upon passive control and safe reinforcement learning fields to learn safe and stable

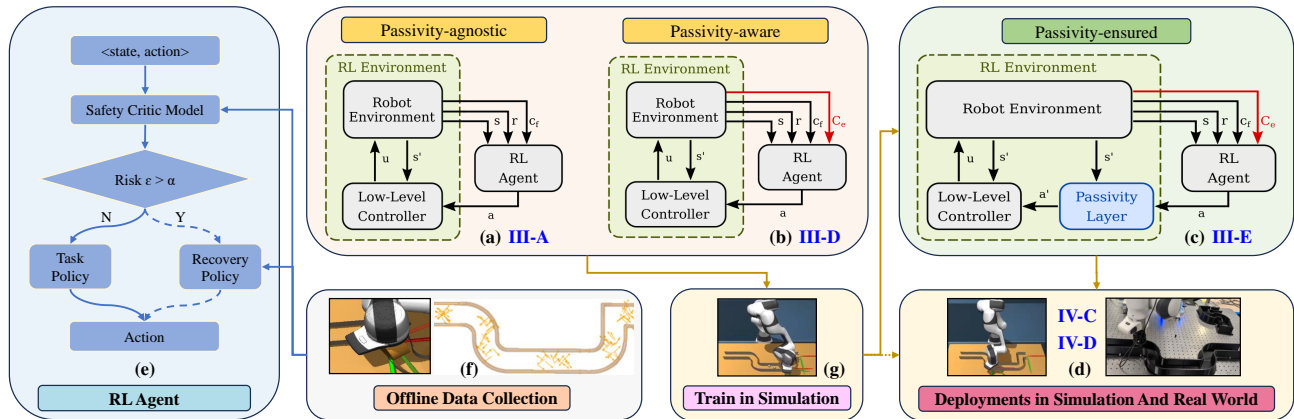


Fig. 1: System overview. The *passivity-agnostic* safe RL framework (a) constitutes the baseline method. We propose a *passivity-aware* policy (b) through energy constraints C_e , and a *passivity-ensured* system (c) by adding a passivity layer to stabilize the RL action. We evaluate these three approaches through simulation and real-world experiments (d). Commonly, in all approaches, the RL agent observes the environment and outputs an action applied to the Cartesian VIC controller (Sec. III-B). The safe RL agent (e) uses a *safety critic* model to detect high risk and switch to the safer *recovery policy*. These models are pre-trained using offline data (f) consisting of random actions executed in multiple areas of the maze. (Sec. IV-B.1). The policy training (g) is completed by online training in simulation (Sec. IV-B.2).

policies for solving contact-rich tasks. As previously mentioned, it uses a passivity-based approach to observe and limit the energy stored in the system such that it can both: 1) impose constraints on the safe RL to train passivity-aware policies (Sec. III-D), and 2) achieve passivity-ensured control by a passivity layer running on the policy output (Sec. III-E). The former approach by itself does not guarantee passivity due to the incompleteness of data and the stochasticity of learning methods. The latter approach provides this guarantee, but can significantly reduce task performance by disrupting the task-oriented policy behavior. We combine both approaches to achieve good task performance while ensuring stability. A diagram of our work is shown in Fig. 1.

A. Safe RL for contact-rich tasks

This section briefly introduces the contact-rich safe RL framework [6] that forms the basis of our proposed method. The problem is formulated as a CMDP [21]. A CMDP can be expressed as a tuple $(\mathcal{S}, \mathcal{A}, R, P, \gamma, \mu, \mathcal{C})$, where \mathcal{S} is the state space, \mathcal{A} is the action space, $R: \mathcal{S} \times \mathcal{A} \rightarrow \mathbb{R}$ is the reward function, P is the state transition probability, $\gamma \in (0, 1)$ is the reward discount factor, μ is the starting state distribution and $\mathcal{C} = \{(c_i: \mathcal{S} \rightarrow \{0, 1\}, \chi_i \in \mathbb{R}) \mid i \in \mathbb{Z}\}$ denotes the constraints that the agent must satisfy. For this specific formalism, we define the state space, action space, reward function, and safety constraints as below. All vectors are in the world reference frame unless specified.

- **State Space \mathcal{S} .** The state space is designed as a 6-dimensional vector for *safety critic* network and *recovery policy* including the wrench $[f_x, f_y, f_z, m_x, m_y, m_z] \in se^*(3)$ measured from an F/T sensor. Additionally, a 9-dimensional state vector is used, which extends this representation by incorporating the end-effector position $[p_x, p_y, p_z] \in \mathbb{R}$.

- **Action Space \mathcal{A} .** Based on [6], we design a 4-dimensional vector as action space, consisting of two end-effector displacement values $[\Delta p_x, \Delta p_y] \in \mathbb{R}$ and 2 stiffness parameters $[K_1, K_2]$. The action dimensions are bounded as listed in Table I. We keep the position Δp_z and stiffness K_z in the z-axis constant. The stiffness values are defined w.r.t. the motion vector $\Delta \mathbf{p}$ with K_1 along the motion vector, K_2 orthogonal to the motion vector and parallel to the ground plane, and K_z normal to the ground plane.
- **Reward Function R .** The agent is penalized for the Euclidean distance between the current position of the end-effector and the goal position multiplied by a constant r_{pos} . High-force collisions are penalized with r_{col} . A bonus is given for reaching the goal r_{goal} to increase convergence speed. The reward multipliers used in our experiments are presented in Table I.
- **Constraints \mathcal{C} .** The force constraint c_f requires the measured force magnitude to stay below a threshold. We also propose two new constraints for passive control, described later in Sec. III-D.

The Safe RL network structure is shown in Fig. 1.e, there are three components in a safe RL agent: Firstly, a *safety critic* model and *recovery policy* are trained with the pre-collected offline data. Then, *task policy* is trained online with the maze exploration task. The policy output as action is given to the VIC, which controls the robot to achieve the desired actions. In the following section, we describe how we apply the RL action with our low-level controller.

B. Cartesian impedance control

The control scheme utilized in this work is a Cartesian VIC, for which the control torques of the impedance term $\tau_{IC}^\top \in \mathbb{R}^n$ are defined in a quasi-static condition as

$$\tau_{IC}^\top = \tau_K^\top - \tau_D^\top, \quad (1)$$

where control torques τ_K^\top are generated by the elastic wrench $\mathbf{w}_K^{0,EE^\top} \in se^*(3)$, which can be expressed as

$$\mathbf{w}_K^{0,EE^\top} = \begin{bmatrix} \mathbf{K}_t & \mathbf{K}_c \\ \mathbf{K}_c^\top & \mathbf{K}_r \end{bmatrix} \Delta\boldsymbol{\eta}. \quad (2)$$

Here, the infinitesimal body twist displacement is described by $\Delta\boldsymbol{\eta} \in se(3)$. The positive definite matrix $\mathbf{K}_c \in \mathbb{R}^{3 \times 3}$ describes the decoupling between the stiffness values of the rotational ($\mathbf{K}_r \in \mathbb{R}^{3 \times 3}$), and translational ($\mathbf{K}_t \in \mathbb{R}^{3 \times 3}$) axes. In this work the values of translational stiffness matrix \mathbf{K}_t are obtained by mapping the RL action stiffness matrix $\mathbf{K}_a = \text{diag}(K_1, K_2, K_z)$ (Sec. III-A) to the world frame as follows $\mathbf{K}_t = \mathbf{R}_p^\top \mathbf{K}_a \mathbf{R}_p$, given

$$\mathbf{R}_p = \begin{bmatrix} \Delta p_x & -\Delta p_y & 0 \\ \Delta p_y & \Delta p_x & 0 \\ 0 & 0 & 1 \end{bmatrix}.$$

The damping related torques are defined as $\tau_D = \mathbf{D}\dot{\mathbf{x}}$, where the damping matrix $\mathbf{D} \in \mathbb{R}^{6 \times 6}$ is formed as in [24] and $\dot{\mathbf{x}} \in se(3)$ is the Cartesian velocity of the end-effector. In the following subsection, we describe the passivity-based approach for guaranteeing the stability of our controller.

C. Passivity-based approach for variable stiffness control

As mentioned in Section I, passivity is a necessity to facilitate physical interactions between a robot and its environment. For an impedance-controlled robot, the energy stored in the system can be expressed as the sum of the storage functions of the controller and robot $S = S_{\text{Ctrl}} + S_{\text{Rob}} \in \mathbb{R}$ [25]. It was shown in [7] that since S_{Rob} is physically bounded, it is also passive. Therefore, the system is passive if and only if the controller described by S_{Ctrl} is passive. Hence, it is a necessity to observe and bound the energy injected by the controller at the power port $(\tau_{\text{Ctrl}}, \dot{\mathbf{q}})$, which is expressed by

$$\dot{S}_{\text{Ctrl}} + P_{\text{IC}} = 0. \quad (3)$$

Here, P_{IC} is expressed as the sum of the energy flows resulting from the spring $P_K = \mathbf{w}_K^{0,EE^\top} \dot{\mathbf{x}} \in \mathbb{R}$ and damping $P_D = \dot{\mathbf{x}}^\top \mathbf{D} \dot{\mathbf{x}} \in \mathbb{R}$. As mentioned previously in Sec. I, one can ensure the passivity of the overall system via the augmentation of the storage function S_{Ctrl} by an energy tank $E_T \in \mathbb{R}$ that is bounded by the upper and lower limits $\bar{E}_T/\underline{E}_T \in \mathbb{R}$. Thus, the energy flow at the power port $(\tau_{\text{Ctrl}}, \dot{\mathbf{q}})$ can be rewritten as follows:

$$\dot{S}_{\text{Ctrl}} + \dot{E}_T + P_D \leq 0, \quad (4)$$

where the energy flow at the tank in this work is defined as $\dot{E}_T = -P_K$. The system passivity requires that the *tank condition* $\underline{E}_T \leq E_T + \dot{E}_T \leq \bar{E}_T$ to always hold.

However, as pointed out in [13], satisfying the *tank condition* is not enough to ensure the passivity of a system, but it is also a necessity to restrict the energy flow \dot{E}_T between the controller and robot. This can be achieved by introducing a flow limit $\dot{E}_T \in \mathbb{R}$, and ensuring that the *flow condition* $\underline{E}_T \leq E_T$ always holds.

In sections III-D and III-E, we go into more detail on how we incorporate *tank* and *flow conditions* into the learning and deployment phases, respectively.

D. Passivity-aware safe RL

This section describes how we add passivity awareness to the RL policy. As described in Section III-A, the safe RL framework achieves safety through constraint definitions. We extend the CMDP formulation by including the passivity constraints so that the safety critic also learns the concept of passivity. As illustrated in Fig. 1.b, this information is provided as the *energy constraints* $C_e \subset \mathcal{C}$, including a budget constraint $c_{eb} \in C_e$ and a flow constraint $c_{ef} \in C_e$, which correspond to the *tank* and *flow conditions*. The budget constraint c_{eb} is introduced to make the agent aware of the amount of energy it has available for adapting the Cartesian stiffness \mathbf{K} during the task. The constraint is triggered whenever $E_T + \dot{E}_T \leq \underline{E}_T$, which indicates that the lower bound of the energy tank is reached.

Whereas the purpose of introducing the energy flow constraint c_{ef} is to make the agent aware of how much energy it is allowed to take out of the tank at any given time for a specific task. Therefore c_{ef} is triggered whenever the draining energy flow of the energy tank exceeds the defined threshold $\dot{E}_T < \underline{E}_T$. RL training episodes are terminated when a constraint happens. This makes it easy to end an episode with both of the energy constraints, hindering the training process. Thus, we experiment with different combinations of these constraints as detailed in Sec. IV. Defining the passivity information as constraints means that the training data includes this information. This data is used to train the safety critic, which learns the risk related to passivity. Therefore, we expect the passivity-aware RL agent to learn to use the energy more economically, in means of cumulative energy spent and instant energy flow. However, learning a regression model does not guarantee that the risk is always predicted correctly. Thus, we recommend deploying these models with the added passivity layer for passivity-ensured control, as described in the following section.

E. Passivity-ensured control

We employ a passivity layer at the output of the RL agent to guarantee the control passivity, as illustrated in Fig. 1.c. The passivity layer contains two filtering actions to satisfy the *tank* and *flow conditions* defined in Section III-C. We ensure the *flow condition* [13] by limiting the rate at which the controller can inject energy into the system through the introduction of the scaling variable

$$\alpha = \begin{cases} \frac{\dot{E}_T}{\underline{E}_T} & \text{if } \dot{E}_T < \underline{E}_T \leq 0 \\ 1 & \text{otherwise.} \end{cases} \quad (5)$$

It is defined as the ratio between the maximal allowed energy flow \underline{E}_T and the originally calculated flow \dot{E}_T , resulting in a new formulation of the energy flow

$$\dot{E}_T' = \begin{cases} \alpha \dot{E}_T & \text{if } \underline{E}_T \leq E_T + \dot{E}_T \leq \bar{E}_T \\ 0 & \text{otherwise.} \end{cases} \quad (6)$$

Integrating the described energy tank dynamic for the VIC, the change of the Cartesian stiffness can be defined as

$$\mathbf{K}(t) = \begin{cases} \mathbf{K}(t-1) & \text{if } E_T + \dot{E}_T' \leq \underline{E}_T \\ \mathbf{K}(t) & \text{otherwise.} \end{cases} \quad (7)$$

In the event that the energy tank becomes depleted, \mathbf{K} is hindered from increasing further, thereby keeping \mathbf{K} constant. This results in a standard Cartesian impedance controller with constant gains. However, when $E_T > \bar{E}_T$ becomes true through a decrease of \mathbf{K} , the change of stiffness is applied but without storing more energy in the tank. In order to enforce the energy flow constraint, α is incorporated in the torques generated by the impedance control term:

$$\boldsymbol{\tau}_{IC}^\top = \alpha \mathbf{J}^\top(\mathbf{q})(\mathbf{w}_K^{0,EE^\top} + \mathbf{D}\dot{\mathbf{x}}). \quad (8)$$

These filtering actions are necessary to guarantee passive behavior. However, reconsidering Fig. 1.c, the RL agent perceives the low-level control and the passivity layer as part of the environment, because these are not part of the RL-based decision-making. Thus, any post-processing applied to the RL action decreases the transparency of the system, i.e., the outcome of the same action may be different depending on the filter variables. For this reason, we combine the passivity layer with passivity-aware policies and evaluate the effects of each component in our experiments.

IV. EVALUATION

We evaluate our method through the contact-rich maze exploration task. In this task, the robot has to explore an unknown maze blindly. Thus, it relies on the force sensing for finding its way out, making it a highly contact-rich task, i.e., the robot cannot avoid contact and it has to regulate the exerted wrenches for safety. In the following evaluation experiments, we aim to study: 1) the passivity from an energy tank perspective during policy learning; 2) how passivity constraints affect RL policy training and performance; 3) how to guarantee both safe and stable performance while executing the task efficiently.

We conduct three types of experiments to study these points. First, we train the agent with different energy tank and energy flow constraints, and compare them to the baseline training that is agnostic to passivity (Sec. IV-B). Second, we deploy the learned models with the addition of the passivity layer in the control loop as shown in Fig. 1 (Sec. IV-C). The passivity layer guarantees control stability by limiting the actions of the agent. Our goal is to understand the trade-off between safety and performance in scenarios that are aware or agnostic of the passivity constraints. Third, we deploy the passivity-integrated approach in a real-world contact-rich robotic task to validate the applicability of our approach (Sec. IV-D).

In the following text, we first describe our experiment setup, then we present the details and results of these three experiments in the three subsequent sections.

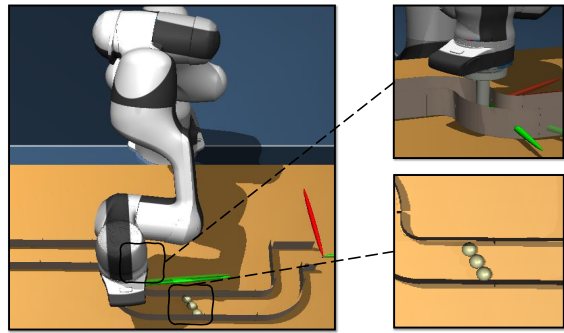


Fig. 2: Experiments setup in MuJoCo. Right top: the robot explores the turn area with contact. Right bottom: three sphere obstacles.

TABLE I: Experiment parameters

Reward multipliers		
$r_{pos} = -400$,	$r_{col} = -250$,	$r_{goal} = 1000$
Action space		
$\Delta p_x, \Delta p_y \in [-3, 3]$ cm,	$K_1, K_2 \in [300, 1000]$ N/m	
Control parameters		
$K_z = 750$,	$\mathbf{K}_r = \text{diag}(100, 100, 0)$, $\mathbf{K}_c = \mathbf{0}$ N/m	
Training hyperparameters		
learning rate: 3×10^{-4} , $\gamma: 0.9$, $\gamma_{safe}: 0.85$, $\epsilon_{risk}: 0.65$		

A. Experiment setup

The experimental task is maze exploration through interaction, where the end-effector trajectories and stiffness values adapt dynamically. We train the policy in simulation using a Mujoco (version 2.3.3) maze environment, adapted from previous work [6], as shown in Fig. 2. The objective is to navigate through the maze only by relying on contact forces, moving from the start point on the left to the goal point on the right. During this process, the controller dynamically adjusts Cartesian stiffness and pose in response to disturbances, such as maze walls and movable obstacles represented by three simulated sphere balls in the middle of the maze. We train the policy on the cluster (1× NVIDIA Tesla V100 16Gb GPU, 1× Intel(R) Xeon(R) Silver 4210 CPU)¹. For the real-world experiment setup please refer to IV-D.

B. Passivity-aware policy training

We run budget-constrained and combined budget-flow-constrained passivity-aware training. We denote the budget-constrained runs as $E_b\theta_b$ and the combined constraint runs as $E_b\theta_b - E_f\theta_f$, where θ_b is the tank size and θ_f is the flow limit times 10 for brevity. In our experiment, we test different energy budgets E_b and flow limits E_f . We evaluate energy budgets in the range of 4–10 and flow limits from -0.7 to -0.3 , based on our preliminary trials.

We also train the *passivity-agnostic* approach as the baseline (*agnostic*) without any energy-based constraints but only with contact-force constraint as shown in Fig. 1, thus the task is more easily achieved during training, however, the policy stays unaware of system stability.

¹We gratefully acknowledge the Data Science and Computation Facility and its Support Team at Fondazione Istituto Italiano di Tecnologia.

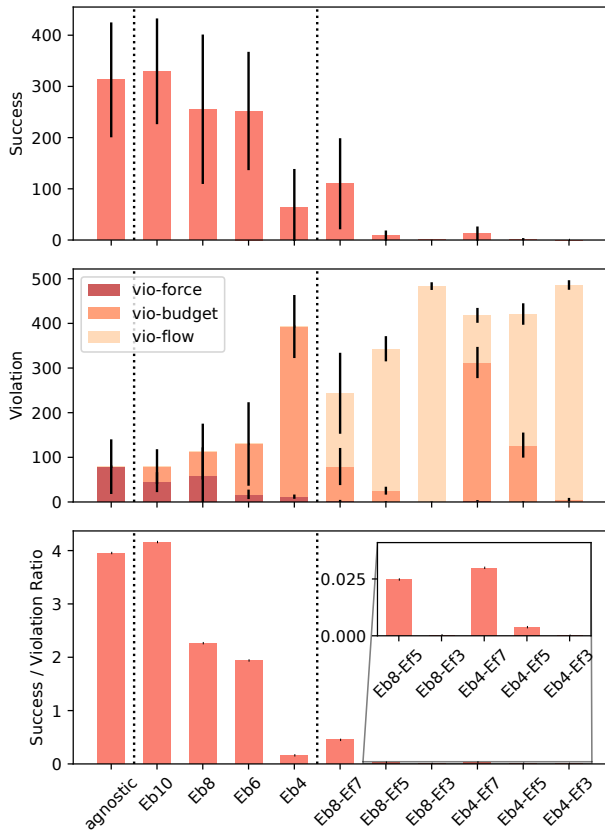


Fig. 3: Passivity-aware policy training experiment results. We present the total numbers of success and violation in the first two plots. The third plot shows the ratio of mean success to mean violation. We zoom into the last 5 case results as they are almost invisible.

1) *Offline data collection:* We collected 40,000 tuples using the same method as in [6], each consisting of $[s, a, s_{t+1}, mask]$ as offline data, where *mask* indicates a constraint violation. In total, there are 1363 constraint violations. In comparison to [6], we increased the force threshold to 40 N (same as in [26]) in this study to better focus on the passivity-based constraints.

2) *Online training:* We first train a passivity-agnostic policy where the agent focuses on safe task completion but is agnostic to system stability. For comparing it to the passivity-aware policies where the budget and energy flow constraints are added during training. These energy constraints, along with the contact force constraint, constitute three distinct constraints as part of CMDP. We trained policies through SAC [27] (see the basic hyper parameters in Tab. I) under different constraint configurations. To minimize random error and statistical bias, we train each policy under various constraint configurations using 10 different random seeds.

3) *Results:* The results of the training experiments are summarized as means and standard deviations of 10 seeds in Fig. 3. As the most relaxed configuration, *agnostic* solves the task earlier than others. We see a consistent increase in constraint violations as the budget size decreases and harsher flow limits are applied. Flow constraints dominate the type

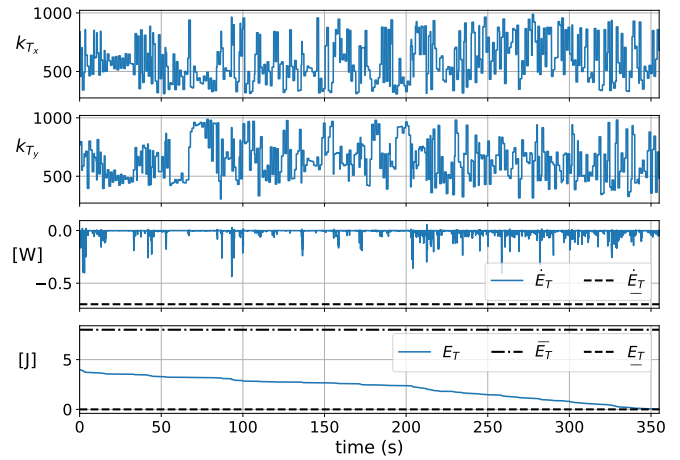


Fig. 4: These plots visualize the effect that the changes of the stiffnesses $k_{T_x}, k_{T_y} \in \mathbf{K}$ during training, have on the energy flow \dot{E}_T and consequently on the energy stored in the tank E_T .

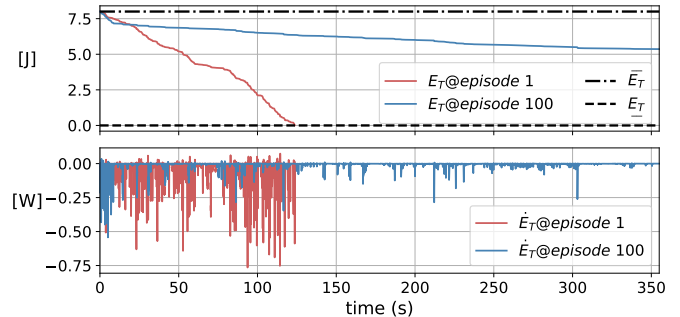


Fig. 5: Plots illustrate the effect that the introduction of the *tank constraint* has on the agents energy expenditure at different stages during training.

of violations as in Eb8 against Eb8-Ef7. These findings suggest that the passivity-constrained cases would benefit from further training.

During training as well as deployment, the agent regulates the stiffness of the impedance controller (Sec. III-B). This has a direct effect on how the energy flow \dot{E}_T and the tank budget E_T , which can be seen in Fig. 4. More specifically, it can be seen that whenever the agent increases the stiffness of springs during its motion, it results in $\dot{E}_T < 0$ as long as $\underline{E}_T \leq E_T < \bar{E}_T$ holds as described in Sec. III-C. Furthermore, it can be observed that the greater the increase in stiffness during a particular motion the greater effect it has on \dot{E}_T and consequently on E_T . This behavior can be directly related to the definition of \dot{E}_T (Sec. III-C). During training, it can be observed how the agent becomes more aware of the effect the changes of \mathbf{K} has on the either \dot{E}_T and/or E_T depending on the constraints it is subjected to.

We present the impact of *energy constraints* in passivity-aware policy training in Fig. 5, showing the agent's energy expenditure at two different stages during training. Specifically, the red graph is the energy expenditure and the energy flow at the port of the tank in the first episode, in other words it has not learned to adapt to this constraint. The blue

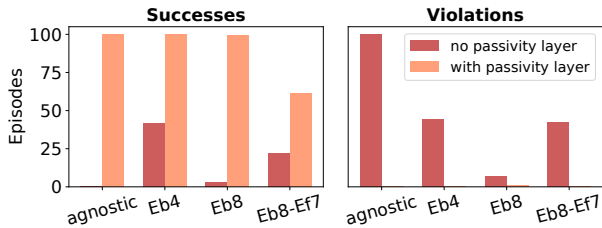


Fig. 6: Policy performance in deployment experiments. The bars show how the models (agnostic, Eb4, Eb8, Eb8-Ef7) perform in terms of successes and violation with and without the passivity layer in simulation for 100 episodes, subjected to the same constraints $\bar{E}_T=6$, $\dot{\bar{E}}_T=-0.5$.

TABLE II: Results of model tests. Performance evaluation over 100 episodes for each of three randomly selected seeds.

Run config.	Violations			Successes
	Force	Tank	Flow	$\mu \pm \sigma$
agnostic	0	0	0	100 \pm 0
Eb4	0	26	0	91.3 \pm 3.9
Eb8	2	0	0	99.3 \pm 0.9
Eb8-Ef7	0	7	0	62 \pm 40.1

graph represents the agent’s energy-related behavior after 100 episodes, making it evident that the agent has learned to act more conservatively, resulting in reduced and more evenly distributed energy expenditure. Hence, it can be seen how introducing the *energy constraint* has a direct impact on the agent’s behavior during training.

After training, we test our policy on representative experiments, including agnostic, Eb4, Eb8, Eb8-Ef7, for comparison. First, all policies are evaluated over 100 episodes under the same constraint settings used during training. The testing results, shown in Table II, demonstrate the model’s strong performance under conditions consistent with its training environment. Notably, the agent achieves a 100% success rate when it is agnostic to energy constraints, as it is not subjected to C_e and can therefore operate more exploitatively during its runs. Furthermore, a comparison between Eb8 and Eb4 reveals that the more conservative tank size in Eb4 consequentiality results in more tank violations. Additionally, it can be seen that the combination of both tank and flow constraints (Eb8-Ef7) results in overall worse performance.

C. Passivity-ensured deployment

In the deployment experiments, we evaluate the effect of the passivity layer on the trained models, by comparing the performances of the *passivity-agnostic* baseline and various *passivity-aware* approaches in combination with and without the passivity layer. In these experiments, we do not retrain the models but impose the passivity layer on the output of the RL agent (Fig. 1), where the layer is with uniform parameter settings: an initial energy budget of $\bar{E}_T=6$ and an energy flow limit of $\dot{\bar{E}}_T=-0.5$.

The results in Fig. 6 showcase the task successes, and violations. Please note that violations here only indicate

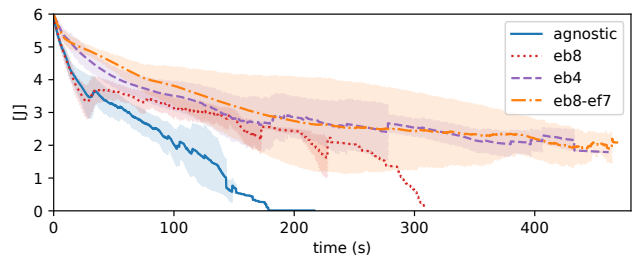


Fig. 7: Energy budget progress during passivity-ensured deployment experiments. The curves indicate the mean of 300 runs (100 per seed) and the shades indicate the standard deviation. Although the passivity-agnostic agent is kept stable by the passivity layer, it shows no awareness of energy expenditure.

force violations. No energy constraint violation happens because of the passivity layer. Overall, the results labeled as “with passivity layer” outperform the baseline labeled as “no passivity layer” in Fig. 6. These results reveal the risks of deploying models without passivity guarantees, leading to system instability and unsafe behaviors despite good performance in model tests shown in Table II. Specifically: i) The agnostic policy performs the worst when no passivity filter is applied, as it consistently violates the flow constraint. Although it achieves a 100% success rate when evaluated without considering energy constraints shown in Table II, which highlights the necessity of incorporating passivity during training. ii) The success rate improves significantly when the passivity filter is applied underscoring the dual benefits of passive-aware policies and the passivity layer, ensuring safer and more stable deployments.

We also present the energy usage of each method in Fig. 7 to further demonstrate the benefit of passivity-aware training. Even though all of agnostic, eb8 and eb4 show full success in the tests (Fig. 6), analysis of the energy budget progress in these runs reveals that the agnostic model depletes its budget rapidly. This rapid depletion reduces its likelihood of success in more complex task instances. On the other hand, eb4 demonstrates the best success and energy efficiency, despite its delayed learning shown in Fig. 3.

D. Real-world experiments

We deploy the trained passivity-aware models in the real world to complete our validation. In real-world experiments as shown in Fig. 8, we implement our method on a Franka Panda robot arm with a flange mounted at the end effector with an ATI45 FT sensor to percept external force and torque, with our passivity-ensured impedance controller (work frequency 1000Hz). We deploy the best models of Eb4, Eb8 and Eb8-Ef7 in the real world without fine-tuning. The robot can finish the task without violating force constraints and energy constraints in each experiment, which validates our method’s effectiveness. However, failure case happened in the passivity-agnostic model as shown in Fig. 8.d. The video is available as supplementary material.

V. CONCLUSION AND FUTURE WORK

In this letter, we investigated the safety and stability of the robotic system under multiple constraints for a contact-

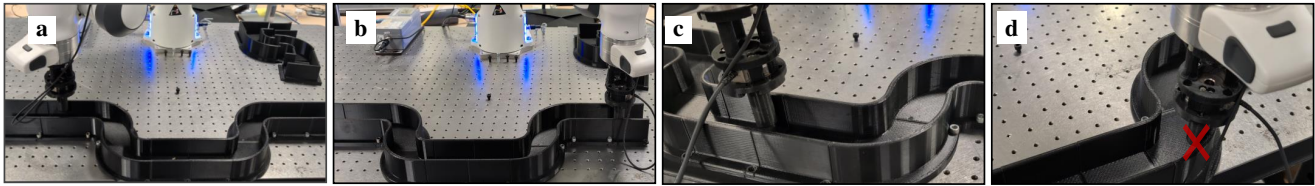


Fig. 8: Snapshots in Real-world Experiments.(a) the overview of maze exploration task, at start point. (b) end of task. (c) closeup robot moves along with contact force and executes at the turnaround area. (d) failure case. violation at turnaround areas, where the robot tries to keep stable and safe but too conservatively.

rich task, demonstrating that the traditional RL approach can not guarantee passivity. Furthermore, we combined an augmented energy tank-based passivity formalism in a safe RL framework. We employed the passivity constraints in both training and deployment of the RL model. The proposed method completed the task without any force and energy constraint violation. Additionally, passivity-aware policies showed improved energy efficiency in deployment, even though they converged later in the training. A set of experiments both in simulation and in the real world on a 7-DoF Franka robot arm validated the effectiveness of the proposed method. We are planning to explore self-adaptive tank-size and flow constraints in the future works.

REFERENCES

- [1] C. Tang, B. Abbatematteo, J. Hu, R. Chandra, R. Martín-Martín, and P. Stone, “Deep reinforcement learning for robotics: A survey of real-world successes,” *Annual Review of Control, Robotics, and Autonomous Systems*, vol. 8, 2024.
- [2] L. Brunke, M. Greeff, A. W. Hall, Z. Yuan, S. Zhou, J. Panerati, and A. P. Schoellig, “Safe learning in robotics: From learning-based control to safe reinforcement learning,” *Annual Review of Control, Robotics, and Autonomous Systems*, vol. 5, pp. 411–444, 2022.
- [3] S. Choi, S. Ha, and W. Kim, “A multi-task energy-aware impedance controller for enhanced safety in physical human-robot interaction,” *IEEE Robotics and Automation Letters*, vol. 10, no. 2, pp. 1345–1352, 2025.
- [4] H. Bharadhwaj, “Auditing robot learning for safety and compliance during deployment,” in *Conference on Robot Learning*. PMLR, 2022, pp. 1801–1806.
- [5] B. Thananjeyan, A. Balakrishna, S. Nair, M. Luo, K. Srinivasan, M. Hwang, J. E. Gonzalez, J. Ibarz, C. Finn, and K. Goldberg, “Recovery rl: Safe reinforcement learning with learned recovery zones,” *IEEE Robotics and Automation Letters*, vol. 6, no. 3, pp. 4915–4922, 2021.
- [6] H. Zhang, G. Solak, G. J. G. Lahr, and A. Ajoudani, “Srl-vic: A variable stiffness-based safe reinforcement learning for contact-rich robotic tasks,” *IEEE Robotics and Automation Letters*, vol. 9, no. 6, pp. 5631–5638, 2024.
- [7] S. Stramigioli, “Energy-aware robotics,” in *Mathematical Control Theory I*, M. K. Camlibel, A. A. Julius, R. Pasumarthy, and J. M. Scherpen, Eds. Cham: Springer International Publishing, 2015, pp. 37–50.
- [8] J. Lachner, F. Allmendinger, S. Stramigioli, and N. Hogan, “Shaping Impedances to Comply With Constrained Task Dynamics,” *IEEE Transactions on Robotics*, vol. 38, no. 5, pp. 2750–2767, Oct. 2022.
- [9] Y. Michel, C. Ott, and D. Lee, “Safety-Aware Hierarchical Passivity-Based Variable Compliance Control for Redundant Manipulators,” *IEEE Transactions on Robotics*, vol. 38, no. 6, pp. 3899–3916, Dec. 2022.
- [10] S. Hjorth, E. Lamon, D. Chrysostomou, and A. Ajoudani, “Design of an energy-aware cartesian impedance controller for collaborative disassembly,” in *2023 IEEE International Conference on Robotics and Automation (ICRA)*, 2023, pp. 7483–7489.
- [11] J. Hathaway, A. Rastegarpanah, and R. Stolkin, “Learning Robotic Milling Strategies Based on Passive Variable Operational Space Interaction Control,” *IEEE Transactions on Automation Science and Engineering*, pp. 1–14, 2023.
- [12] R. Zanella, G. Palli, S. Stramigioli, and F. Califano, “Learning passive policies with virtual energy tanks in robotics,” *IET Control Theory & Applications*, vol. 18, no. 5, pp. 541–550, 2024.
- [13] E. Shahriari, L. Johannsmeier, E. Jensen, and S. Haddadin, “Power flow regulation, adaptation, and learning for intrinsically robust virtual energy tanks,” *IEEE Robotics and Automation Letters*, vol. 5, no. 1, pp. 211–218, 2019.
- [14] Y. Michel, M. Saveriano, and D. Lee, “A Novel Safety-Aware Energy Tank Formulation Based on Control Barrier Functions,” *IEEE Robotics and Automation Letters*, vol. 9, no. 6, pp. 5206–5213, June 2024.
- [15] Í. Elguea-Aguinaco, A. Serrano-Muñoz, D. Chrysostomou, I. Inziarte-Hidalgo, S. Bøgh, and N. Arana-Arexolaleiba, “A review on reinforcement learning for contact-rich robotic manipulation tasks,” *Robotics and Computer-Integrated Manufacturing*, vol. 81, p. 102517, 2023.
- [16] A. Ajoudani, A. M. Zanchettin, S. Ivaldi, A. Albu-Schäffer, K. Kosuge, and O. Khatib, “Progress and prospects of the human-robot collaboration,” *Autonomous Robots*, vol. 42, no. 5, pp. 957–975, 2018.
- [17] C. Chang, K. Haninger, Y. Shi, C. Yuan, Z. Chen, and J. Zhang, “Impedance adaptation by reinforcement learning with contact dynamic movement primitives,” in *2022 IEEE/ASME International Conference on Advanced Intelligent Mechatronics (AIM)*. IEEE, 2022, pp. 1185–1191.
- [18] X. Zhang, L. Sun, Z. Kuang, and M. Tomizuka, “Learning variable impedance control via inverse reinforcement learning for force-related tasks,” *IEEE Robotics and Automation Letters*, vol. 6, no. 2, pp. 2225–2232, 2021.
- [19] Q. Yang, A. Dürr, E. A. Topp, J. A. Stork, and T. Stoyanov, “Variable impedance skill learning for contact-rich manipulation,” *IEEE Robotics and Automation Letters*, vol. 7, no. 3, pp. 8391–8398, 2022.
- [20] R. Martin-Martín, M. A. Lee, R. Gardner, S. Savarese, J. Bohg, and A. Garg, “Variable impedance control in end-effector space: An action space for reinforcement learning in contact-rich tasks,” in *2019 IEEE/RSJ International Conference on Intelligent Robots and Systems (IROS)*. IEEE, 2019, pp. 1010–1017.
- [21] E. Altman, *Constrained Markov decision processes*. Routledge, 1995.
- [22] H. Bharadhwaj, A. Kumar, N. Rhinehart, S. Levine, F. Shkurti, and A. Garg, “Conservative safety critics for exploration,” in *International Conference on Learning Representations*, 2021.
- [23] D. Sacerdoti, F. Benzi, and C. Secchi, “A reinforcement learning-based control strategy for robust interaction of robotic systems with uncertain environments,” in *2024 IEEE International Conference on Robotics and Automation (ICRA)*, 2024, pp. 5788–5794.
- [24] C. Ott, *Cartesian impedance control of redundant and flexible-joint robots*. Springer, 2008.
- [25] J. Lachner, “A geometric approach to robotic manipulation in physical human-robot interaction,” PhD Thesis - Research UT, graduation UT, University of Twente, Netherlands, July 2022.
- [26] X. Zhu, S. Kang, and J. Chen, “A contact-safe reinforcement learning framework for contact-rich robot manipulation,” in *2022 IEEE/RSJ International Conference on Intelligent Robots and Systems (IROS)*. IEEE, 2022, pp. 2476–2482.
- [27] T. Haarnoja, A. Zhou, P. Abbeel, and S. Levine, “Soft actor-critic: Off-policy maximum entropy deep reinforcement learning with a stochastic actor,” in *International conference on machine learning*. PMLR, 2018, pp. 1861–1870.